Constructing a Mimetic Curl using Gauss' Theorem

Eduardo Sanchez, Guillermo Miranda,
and Jose Castillo

November 25, 2014

Publication Number: CSRCR2014-04

Computational Science & Engineering Faculty and Students Research Articles

Database Powered by the Computational Science Research Center Computing Group & Visualization Lab

COMPUTATIONAL SCIENCE & ENGINEERING

SAN DIEGO STATE UNIVERSITY

Computational Science Research Center
College of Sciences
5500 Campanile Drive
San Diego, CA 92182-1245
(619) 594-3430

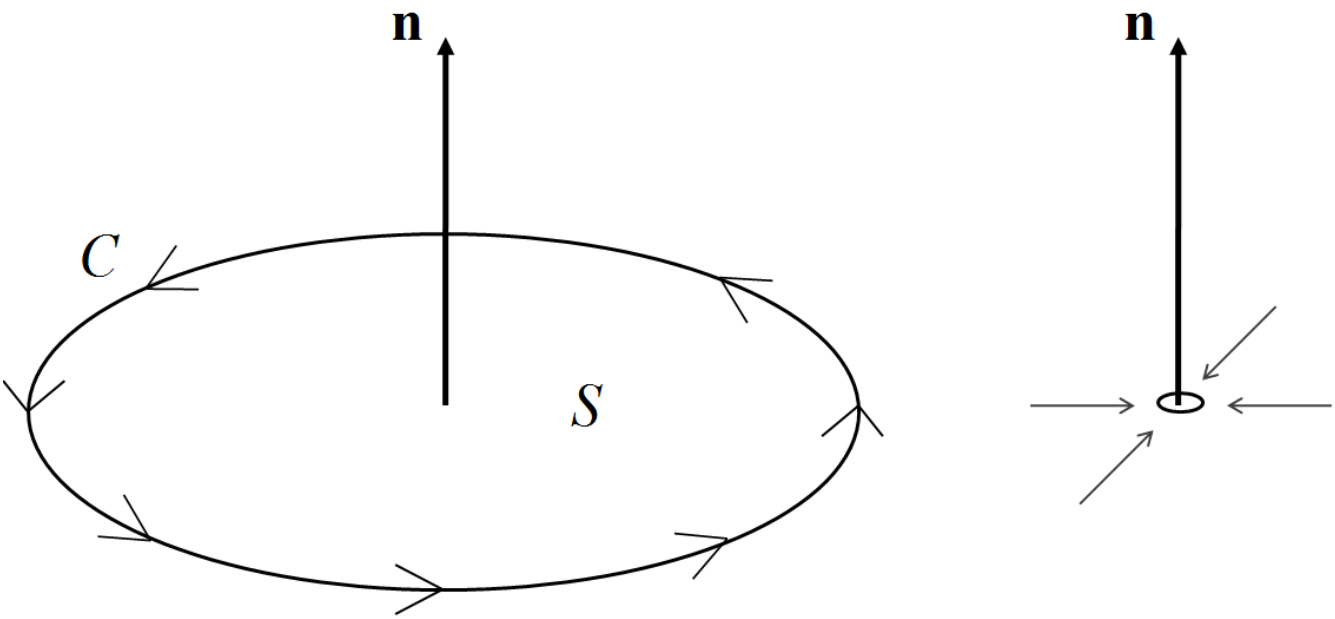

Figure 3. A small rotating disk S, bounded by C, with an orienting normal $\mathbf{n}$. A limiting process then takes place by collapsing the diameter of S to 0, thus allowing for a definition for the curl operator based on Stokian circulation.

Figure 3 summarizes the limiting process used to attain the previous definition.

If S is a 2D rectangle (for example) then C appears as a set of four rectilinear edges for S, and the evaluation of the circulation of v along C needs an estimation for the so called tangential components of $\mathbf{v}$ (Figure 3). This in turn, implies the introduction of dual spaces in the context of the general Stokes' Theorem on manifolds.

In this work, we propose a different approach, so that such introduction becomes unnecessary. We will rely on physical intuition to look at this situation from a different point of view.

2. Mimetic Operators

In this work, we will define a discrete differential operator to be **mimetic**, if and only if it satisfies all of the properties of its continuous counterpart; including approximating the desired solution with a uniform order of numerical accuracy all along the discrete domain of interest (including the boundary).

We will denote a k-th order-accurate (k even and positive), on the (x,y,z), (x,y), or x domains (3, 2, or 1D), mimetic operator as:

1. Mimetic gradient: $\breve{\mathbf{G}}^k_{\{xyz,xy,x\}}$
2. Mimetic divergence: $\breve{\mathbf{D}}^k_{\{xyz,xy,x\}}$
3. Mimetic curl: $\breve{\mathbf{C}}^k_{\{xyz,xy,x\}}$

Mimetic operators are built by means of computing the entries of the stencil so that the resulting matrices satisfy the following theorem [1]:

Theorem 2.1 ***(Extended Gauss Divergence Theorem)*** *Let $f:\mathbb{R}^3 \longmapsto \mathbb{R}$ be a scalar-valued field with continuous first derivatives on some open superset of Ω, let $\mathbf{v}(\mathbf{x}) = p(\mathbf{x})\hat{\mathbf{i}} + q(\mathbf{x})\hat{\mathbf{j}} + r(\mathbf{x})\hat{\mathbf{k}}$, for any $\mathbf{x} \in \mathbb{R}^n$ ($n > 1$), where p, q, and r have continuous first derivatives on some open superset of a solid Ω, and let $\mathbf{n}$ be the outward normal orienting the bounding surface of Ω, $\partial\Omega$, then*

$$\iiint_{\Omega} (\nabla f)\cdot\mathbf{v}dV + \iiint_{\Omega} f(\nabla\cdot\mathbf{v})dV = \iint_{\partial\Omega} (\mathbf{v}\cdot\mathbf{n})fdS \quad (5)$$

Considering a discretized version of the previous results, for an approximation of k-th order of numerical accuracy, leads to:

$$\langle \breve{\mathbf{G}}^k \tilde{f}, \tilde{\mathbf{v}}\Delta x\rangle_{\mathbf{P}} + \langle \tilde{f}, \breve{\mathbf{D}}^k \tilde{\mathbf{v}}\Delta x\rangle_{\mathbf{Q}} \quad = \quad \langle \tilde{f}, \breve{\mathbf{B}}\tilde{\mathbf{v}}\rangle. \quad (6)$$

Castillo and Grone [2] studied and solved an important drawback of the MFDs at the time through the **Castillo–Grone Method (CGM)**. In [3], the author presented a similar approach for constructing mimetic operators, which is then improved in [1]. This second explanation is referred to as the **Castillo–Runyan–Sanchez (CRS) algorithm**. In [3], the author proposes a discretization scheme for the curl operator, based upon the concept of circulation.

Although very descriptive, this proposed discretization requires the interpolation of the argument vector field.

Our goal then is to construct a mimetic curl operator in two and three dimensions, $\breve{\mathbf{C}}^k_{\{xyz,xy\}}$, that profits from the high accuracy up to the boundary exhibited by mimetic divergence operators, without requiring any interpolation [1, 4].

We will revisit the definition for the curl operator, based on Stokes' Theorem, and we will instead construct the curl operator using Theorem 2.1.

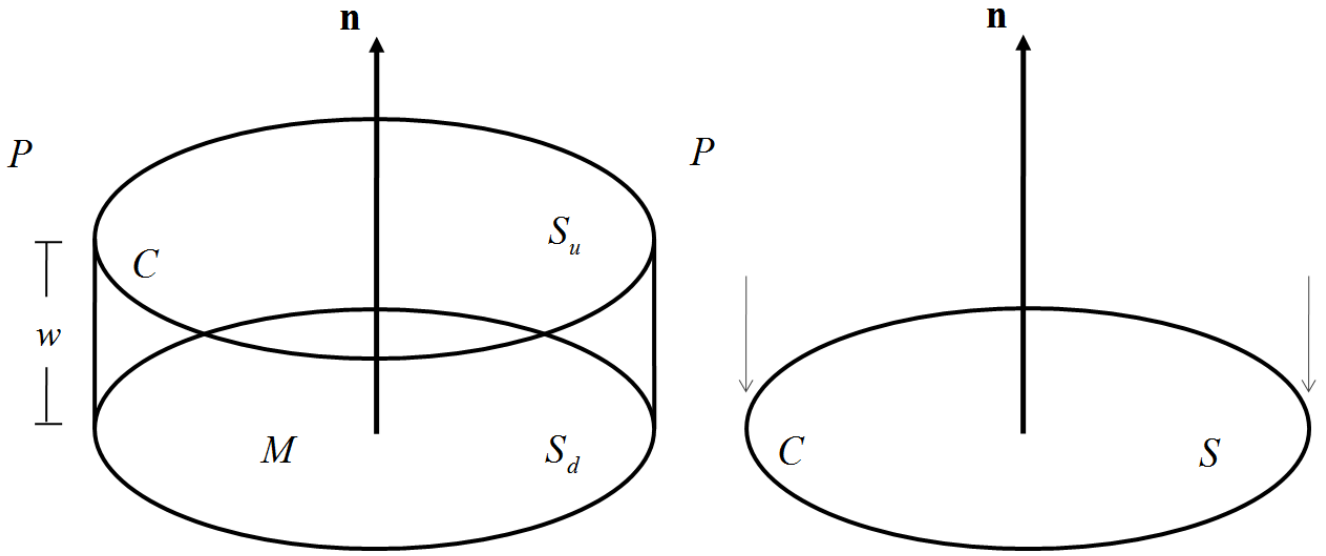

Figure 4. A limiting process for an infinitesimally thin disk S with boundary C and orienting normal $\mathbf{n}$ created upon collapsing surfaces S_u and S_d, aligned through a mantle M of width w, which is then considered to tend to 0.

3. Redefining the Curl Through Gaussian Fluxes

Mathematically, a closed circuit such as C is a 1D object, and can be thought of as modeling a 3D thin wire having a cross-section with an infinitely small diameter, thus collapsing its three-dimensionality to only one dimension. In fact, this was Faraday's view when he formulated mathematically his experimental magnetic induction Law observed in electric circuits [5].

But there is an alternative way for collapsing a 3D object down to a 2D object having a 1D boundary C. Instead of a 2D plane surface S with oriented normal $\mathbf{n}$, think of a thin three-dimensional cylindrical plate, with cylindrical axis along $\mathbf{n}$, and having S as uniform cross-section. If this 3D cylindrical plate becomes infinitely thin, then it becomes a 2D surface with 1D boundary C, but now C is regarded as an object which is a limiting form for a 2D band or cylindrical mantle M, through which some vector field can flow, and some flux can be computed there. This mantle M, together with two surfaces parallel to S, to wit S_u above S, and S_d below S, S_u and S_d having the same area $A(S)$, and being very close to one another, constitute the total surface boundary of a 3D thin plate P (Figure 4).

Naturally, should we consider some 3D vector field which is normal to $\mathbf{n}$, and therefore, also parallel to S_d and S_u, then its Gaussian flux through the boundary of P would reduce to the flux through its mantle M. Since M is a 2D band, with a width w equal to the distance between the parallel surfaces S_d and S_u (Figure 5).

It follows that when w tends to zero, S_d and S_u collapse to S, and the 2D band M collapses to the 1D closed circuit C (see Figures 4 and 5).

This visualization of geometric dimensional collapse will allow us, in the next section, to numerically estimate the scalar components of a 3D curl vector field from some adequate 2D fluxes, rather than from 1D circulations . This will be possible by means of some auxiliary 2D vector fields. In turn, these 2D fluxes will be related to Castillo–Grone 2D mimetic divergence operators.

3.1 Auxiliary 2D Vector Fields

The basic definitions have already been described in [4], and we transcribe them here with some notational changes. There, the type of 2D staggering needed in order to compute the 2D curl, is worked out in detail, but the combination of simultaneous staggerings in the x, y and z-directions needed in the 3D case, is only hinted at graphically (See Figure 4.10 in [4]). In the present work, a more detailed presentation is given.

These auxiliary vector fields, will be defined as follows. If:

$$\text{curl } \mathbf{v} = \mathbf{i}\left(\frac{\partial r}{\partial y} - \frac{\partial q}{\partial z}\right) + \mathbf{j}\left(\frac{\partial p}{\partial z} - \frac{\partial r}{\partial x}\right) + \mathbf{k}\left(\frac{\partial q}{\partial x} - \frac{\partial p}{\partial y}\right), \tag{7}$$

then, for the 3D vector field $\mathbf{v}$, we define the following three 2D auxiliary vector fields:

$$\mathbf{v}^*_{xy} = \mathbf{v}\times\mathbf{k} = \mathbf{i}q - \mathbf{j}p = \mathbf{i}P^*_{xy} + \mathbf{j}Q^*_{xy} \tag{8}$$

$$\mathbf{v}^*_{yz} = \mathbf{v}\times\mathbf{i} = \mathbf{j}r - \mathbf{k}q = \mathbf{j}Q^*_{yz} + \mathbf{k}R^*_{yz} \tag{9}$$

$$\mathbf{v}^*_{zx} = \mathbf{v}\times\mathbf{j} = \mathbf{k}p - \mathbf{i}r = \mathbf{k}R^*_{zx} + \mathbf{i}P^*_{zx}. \tag{10}$$

From here it follows immediately that:

$$\text{curl } \mathbf{v}(x,y,z) = \mathbf{i}\text{div } \mathbf{v}^*_{yz} + \mathbf{j}\text{div } \mathbf{v}^*_{zx} + \mathbf{k}\text{div } \mathbf{v}^*_{xy}. \tag{11}$$

Therefore, the 3D vector expression for curl $\mathbf{v}$ at some point (x,y,z) depends upon three scalar 2D divergences evaluated at that point. These 2D divergences, simultaneously

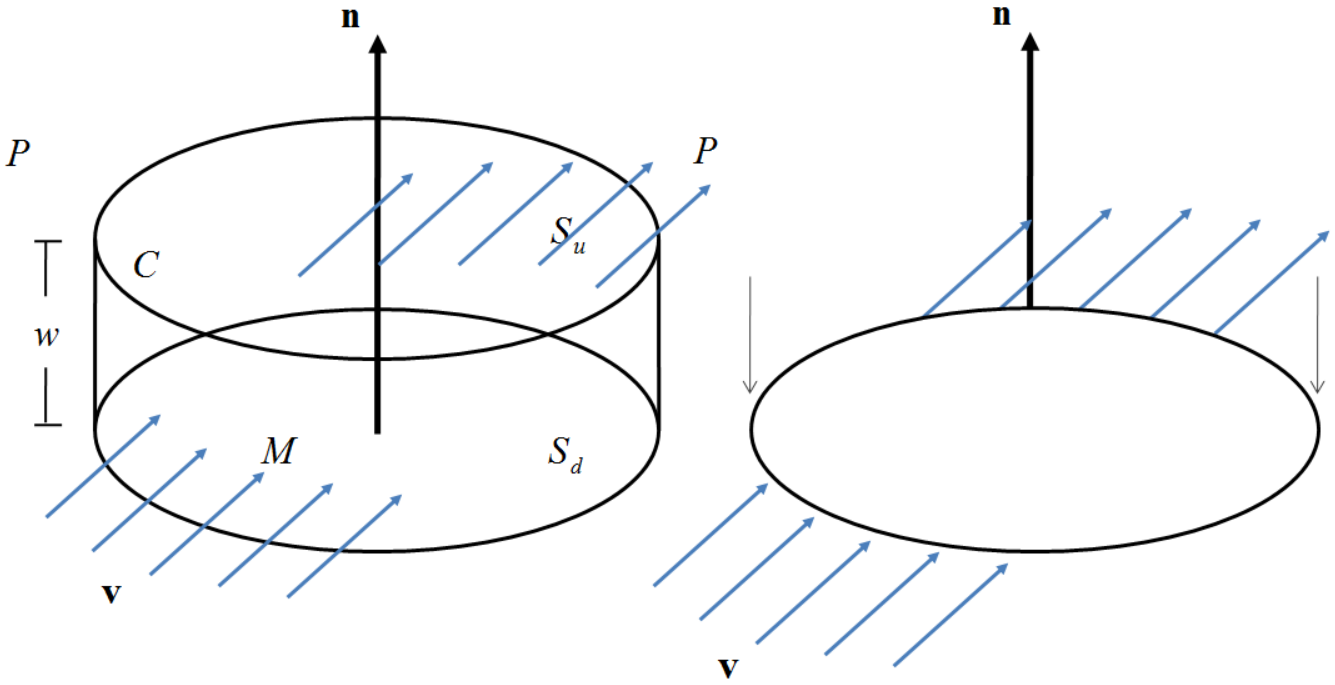

Figure 5. A Gaussian-like flux, through the infinitesimally thin disk S.

needed for our 3D curl $\mathbf{v}$, all arise from 2D fluxes of vectors $\mathbf{v}^*_{yz}$, $\mathbf{v}^*_{zx}$ and $\mathbf{v}^*_{xy}$, and these vector fields lie in planes orthogonal to the coordinate axis, passing through the point (x,y,z) where curl $\mathbf{v}$ is evaluated (Figure 9).

By its definition, $\mathbf{v}^*_{xy}$ lies in a plane orthogonal to the z-axis, and we have that (for 2D vector fields):

$$< \mathbf{k}, \text{curl } \mathbf{v}(x,y,z) >= \text{div } \mathbf{v}^*_{xy}(x,y,z). \tag{12}$$

Analogously:

$$< \mathbf{i}, \text{curl } \mathbf{v}(x,y,z) > \;=\; \text{div } \mathbf{v}^*_{yz}(x,y,z) \tag{13}$$
$$< \mathbf{j}, \text{curl } \mathbf{v}(x,y,z) > \;=\; \text{div } \mathbf{v}^*_{zx}(x,y,z). \tag{14}$$

As far as the construction of the 2D mimetic operators, if the **natural lexicographical order** is chosen, we can build the 2D counterparts to higher-order mimetic operators, as follows [3]:

$$\breve{\mathbf{G}}^k_{xy} \;=\; \begin{bmatrix} \mathbf{G}_x(k) \\ \mathbf{G}_y(k) \end{bmatrix}, \tag{15}$$
$$\breve{\mathbf{D}}^k_{xy} \;=\; [\mathbf{D}_x(k)\,\mathbf{D}_y(k)], \tag{16}$$

where each auxiliary discretization matrix along each spatial dimension can be computed from the 1D mimetic operator, as follows:

$$\mathbf{G}_x(k) \;=\; \hat{\mathbf{I}}^T_n \otimes \breve{\mathbf{G}}^k_x \tag{17}$$
$$\mathbf{G}_y(k) \;=\; \breve{\mathbf{G}}^k_y \otimes \hat{\mathbf{I}}^T_m \tag{18}$$
$$\mathbf{D}_x(k) \;=\; \hat{\mathbf{I}}_n \otimes \breve{\mathbf{D}}^k_x \tag{19}$$
$$\mathbf{D}_y(k) \;=\; \breve{\mathbf{D}}^k_y \otimes \hat{\mathbf{I}}_m \tag{20}$$

Let us go back to Stokes and Gauss while considering the component of curl $\mathbf{v}$ along the z-axis, i.e., $< \mathbf{k}, \text{curl } \mathbf{v}(x,y,z) >$.

Stokes reads as:

$$\iint < \mathbf{k}, \text{curl } \mathbf{v}(x,y,z) > dxdy = \tag{21}$$
$$\oint (p(x,y,z)dx + q(x,y,z)dy),$$

Now, when $\mathbf{i}dx + \mathbf{j}dy$ is a tangent vector of length ds along a counterclockwise oriented circuit C_{xy} in the x-y Plane, then $\mathbf{i}dy - \mathbf{j}dx$ is a normal field $\mathbf{n}ds$, outwardly directed to C_{xy}, and the previous Stokes' formula can be now read "Gauss-like" as follows:

$$\begin{aligned} \iint (\text{div } \mathbf{v}^*_{xy}(x,y,z))dxdy &= \oint (P^*_{xy}(x,y,z)dy - Q^*_{xy}(x,y,z)dx) \\ &= \oint < \mathbf{i}P^*_{xy} + \mathbf{j}Q^*_{xy}, \mathbf{i}dy - \mathbf{j}dx > \\ &= \oint < \mathbf{v}^*_{xy}(x,y,z), \mathbf{n}(x,y,z) > ds. \end{aligned}$$

Since these expressions also equal the mean value of the quantity $< \mathbf{k}, \text{curl } \mathbf{v}(x,y,z) >$ times the area of the surface surrounded by C_{xy}, then we see that this mean value:

$$\oint < \mathbf{v}^*_{xy}(x,y,z), \mathbf{n}(x,y,z) > ds \tag{22}$$

equals the outward flux of $\mathbf{v}^*_{xy}$ through C_{xy}, divided by the above surface area.

It can then be seen that this approach preserves the original behavior inherent to the functioning of Stoke's theorem. Furthermore, this approach is simple, in the sense that, in its foundation, it is just a change of variables.

4. Spatial Discretization Through Staggered Grids

The 2D space is discretized through a staggered grid, as shown in Figure 6.

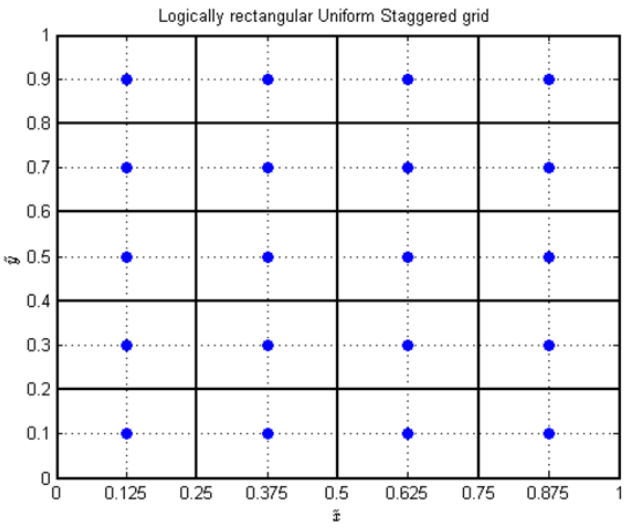

Figure 6. A logically rectangular, 2D uniform staggered grid, as rendered by a visualizer developed by the first author, available in [6].

However, the introduction of the auxiliary vector fields span a shifting on the staggered grid. In the case of a 2D vector field. Figure 7 shows this.

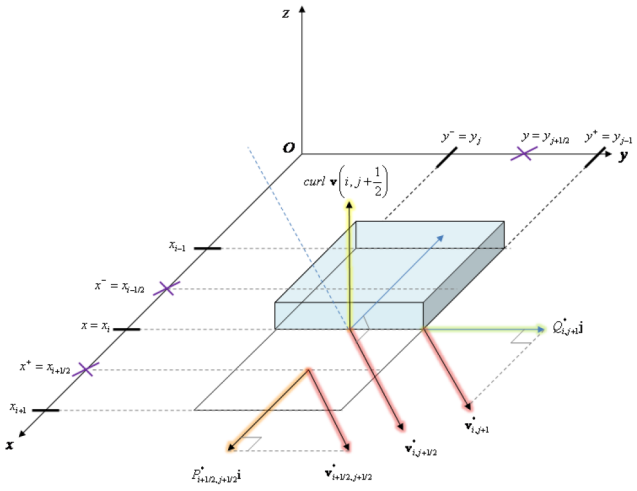

Figure 7. The auxiliary vector fields acting on a 2D domain implicitly define a translation of the grid, thus making up for the interpolation of the original method proposed in [3]. Source of image: [4].

The same occurs in the case of a 3D vector field, as it can be seen in Figure 8. It should be apparent that this implicit translation of the coordinates, makes up for the interpolation previously required.

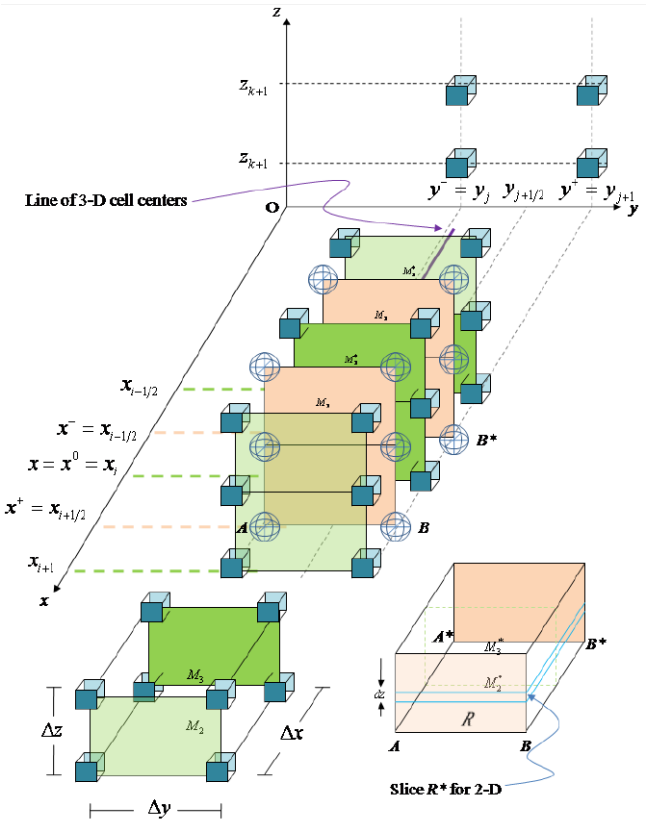

Figure 8. The auxiliary vector fields acting on a 3D domain implicitly define a translation of the grid, thus making up for the interpolation of the original method proposed in [3]. Source of image: [4].

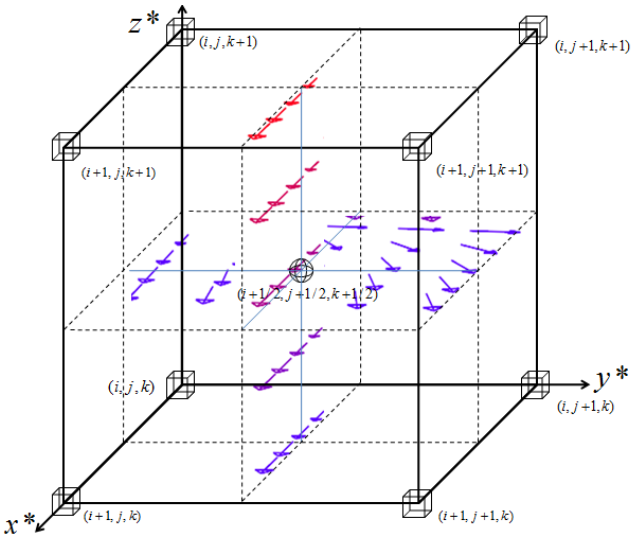

Figure 9. A detailed depiction of two out of three auxiliary fields on a cell of the auxiliary grid, discretizing a 3D vector field.

Figure 9 provides a more detailed depiction of how is each cell (in the auxiliary grid) discretized. Figure 10 provides an intuitive depiction of how is the operator bound to the grid.

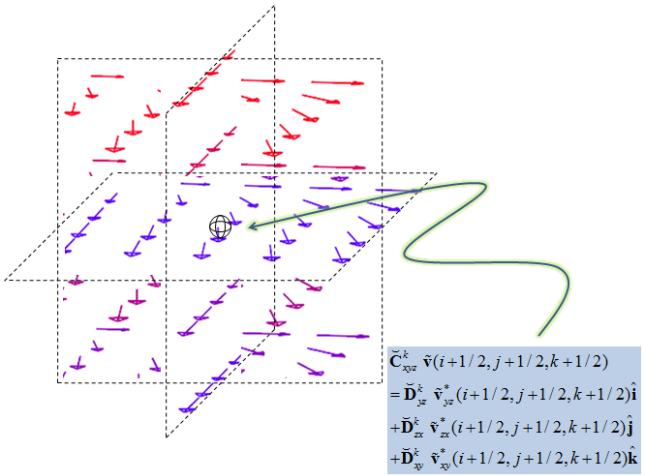

Figure 10. Actual computation of the 3D curl and its binding to the implicitly defined auxiliary staggering.

5. A 2D Test Case Based on the Definition of Angular Motion

Let:

$$\mathbf{v}(x,y,z) = -\mathbf{i}y + \mathbf{j}x. \tag{23}$$

This vector field is plotted in Figure 11.

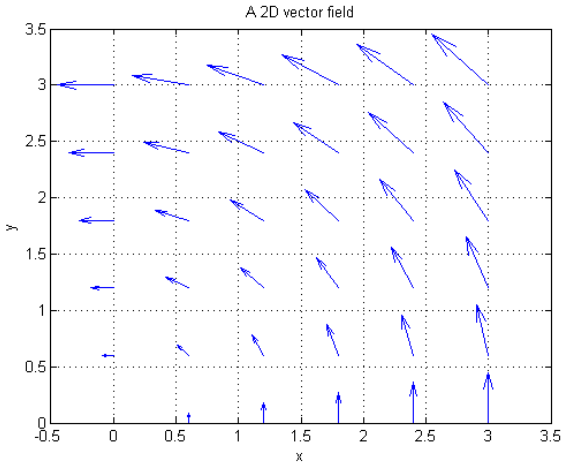

Figure 11. Vector field: $\mathbf{v}(\mathbf{x}) = -y\mathbf{i} + x\mathbf{j}$.

Since $\mathbf{v} = \mathbf{k} \times (\mathbf{i}x + \mathbf{j}y)$, we have $p(x,y,z) = -y$, $q(x,y,z) = x$, and $r(x,y,z) = 0$. In this case, we know that $\mathbf{v} \times \mathbf{k} = \mathbf{i} \times x + \mathbf{j}y = \mathbf{v}^{*}_{xy}(x,y,z)$. Thus, div $\mathbf{v}^{*}_{xy} = 1 + 1 = 2$, which is constant throughout the grid. Figure 12 shows this.

In order to test the correctness of the 2D mimetic divergence, Figure 13 shows a suggested vector field, which is designed based on the test case of interest. This vector field was discretized on a staggered grid, and its divergence was then computed. The results are given in Figure 14.

The suggested vector field, was then discretized, on a staggered grid, and the auxiliary vector fields, were also discretized. Figure 15 plots the auxiliary vector field.

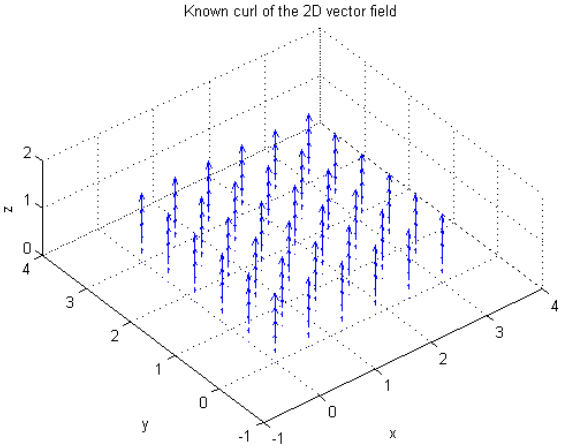

Figure 12. Known curl field: $\nabla \times \mathbf{v} = 2\mathbf{k}$.

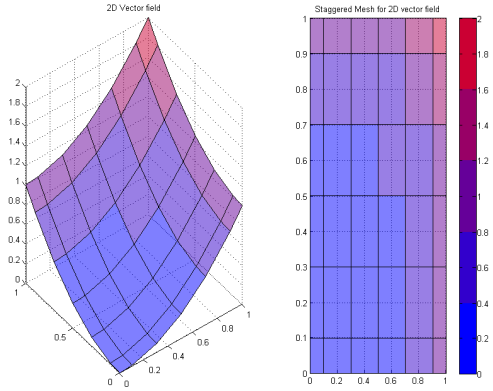

Figure 13. A 2D discretization of the proposed vector field, on a logically rectangular 2D uniform staggered grid, to test the correctness of $\breve{\mathbf{D}}^{2}_{xy}$.

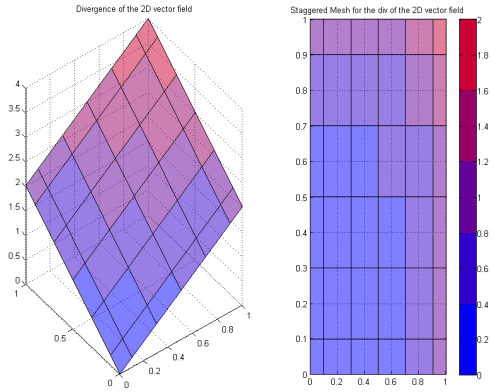

Figure 14. Result of applying $\breve{\mathbf{D}}^{2}_{xy}$.

Figure 16 shows the computed mimetic curl, through the Gaussian approach. This plot has to be compared with that of Figure 12. It should be clear, given the mathematical nature of the selected vector field, that the result is correct.

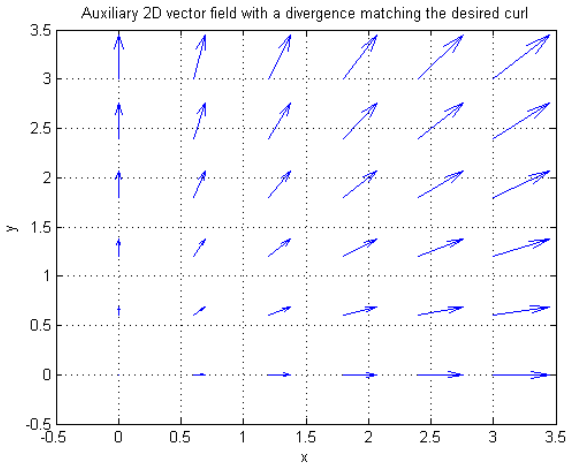

Figure 15. Auxiliary vector field: $\mathbf{v}^*_{xy} = \mathbf{v} \times \mathbf{k}$.

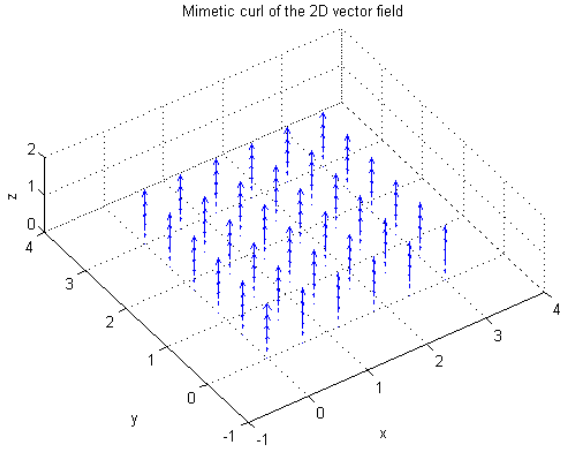

Figure 16. Computed mimetic curl (Gaussian).

6. A Vector Field Modeling Hurricanes

In order for us to try the proposed approach on a model that has physical meaning, we propose the following test case. From [7], a hurricane model that combines a velocity field (counterclockwise vortex flow) around a chosen reference point (e.g. the origin) of strength k, $\mathbf{v}_1(x,y)$, and a uniform sink flow toward the reference point of strength q, $\mathbf{v}_2(x,y)$, is:

$$\mathbf{h}(x,y) = \mathbf{v}_1(x,y) + \mathbf{v}_2(x,y) \tag{24}$$

or

$$\mathbf{h}(x,y) = -\frac{1}{2\pi(x^2+y^2)}[(qx+ky)\mathbf{i} + (qy-kx)\mathbf{j}]. \tag{25}$$

In this work: $q = k = 2\pi$.

Both components, $\mathbf{v}_1$ and $\mathbf{v}_2$ of the proposed model are rendered in Figures 17 and 18. A hurricane model that combines a velocity field (counterclockwise vortex flow) around a chosen reference point (e.g. the origin) is rendered in Figure 19.

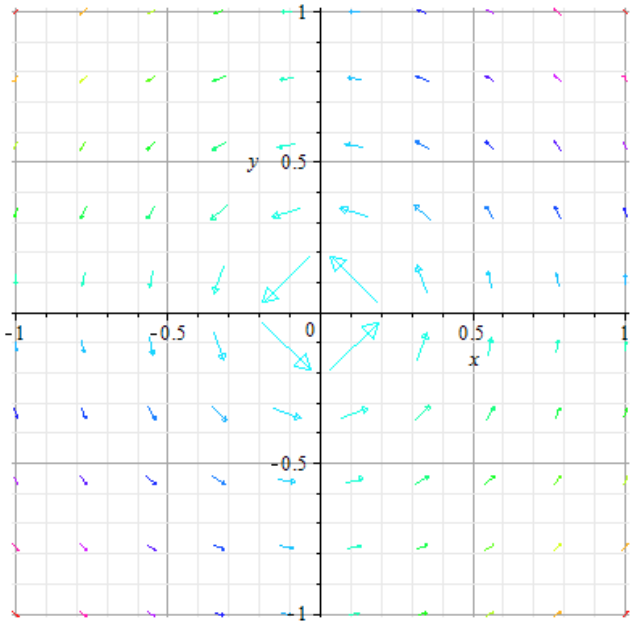

Figure 17. A velocity field $\mathbf{v}_1$ described by a counterclockwise vortex flow.

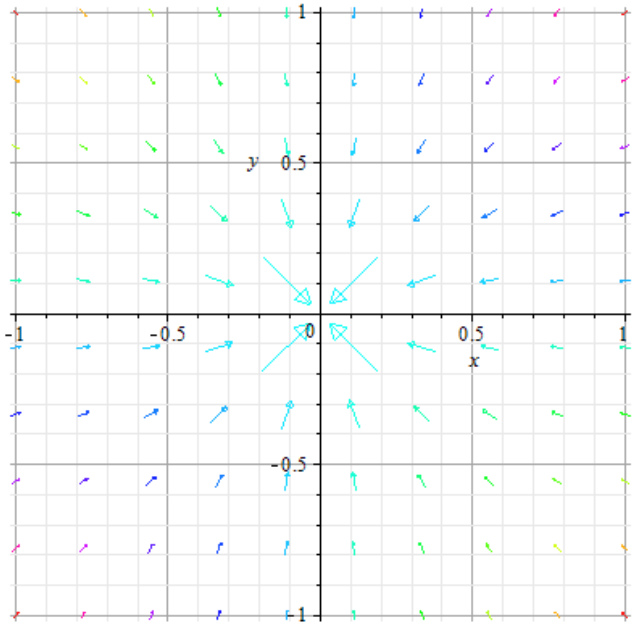

Figure 18. A velocity field $\mathbf{v}_2$ described by a uniform sink flow.

Figure 20 shows first the computed divergence of the proposed 2D field modeling the hurricanes. One can notice, that this particular vector field has an avoidable discontinuity in the origin.

Figure 21 shows the computed curl field. In this context, the importance of the curl is that it allows us to compute the vorticity at any point, defined as

$$\Gamma = 2||\nabla \times \mathbf{h}||. \tag{26}$$

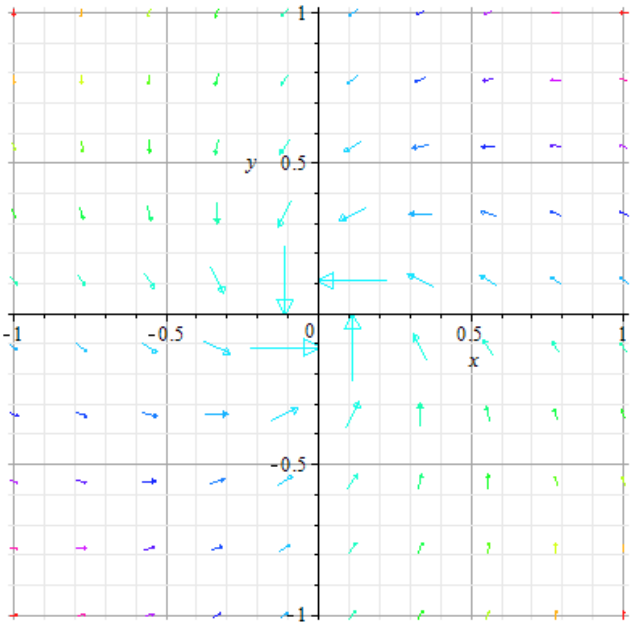

Figure 19. A hurricane model that combines a velocity field (counterclockwise vortex flow) around a chosen reference point (e.g. the origin) of strength k, $\mathbf{v}_1(x,y)$, and a uniform sink flow toward the reference point of strength q, $\mathbf{v}_2(x,y)$.

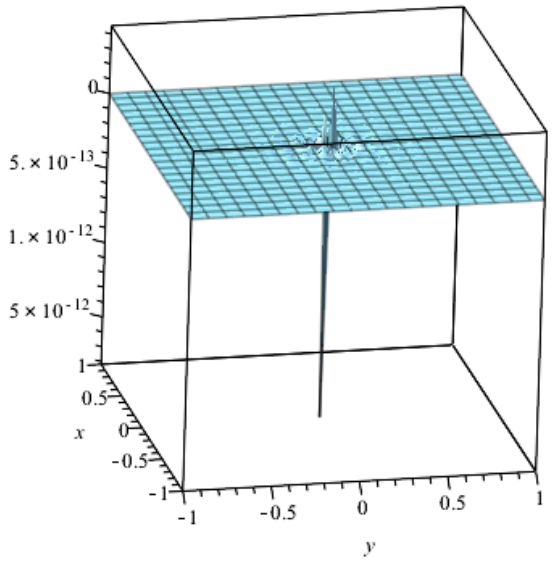

Figure 20. Computed divergence of the hurricane model, i.e. $\nabla \cdot \mathbf{h}$.

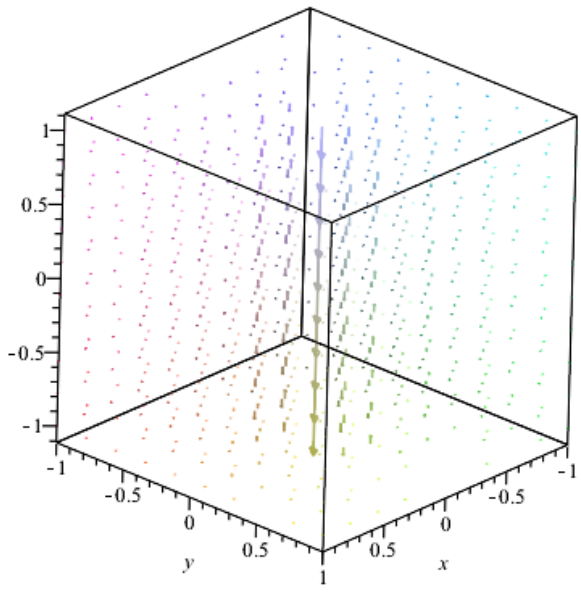

Figure 21. Computed curl of the hurricane model, which allows then to numerically compute the vorticity as $\Gamma = 2||\nabla \times \mathbf{h}||$, across the given domain.

7. Summary, Conclusions, and Future Work

We have presented a new construction of the curl operator, which is compatible with the framework of mimetic operators:

$$\begin{aligned} \check{\mathbf{C}}^k_{xyz}\tilde{\mathbf{v}}(\mathbf{x}) &= \check{\mathbf{D}}^k_{yz}\tilde{\mathbf{v}}^*_{yz}(\mathbf{x})\mathbf{i} + \check{\mathbf{D}}^k_{zx}\tilde{\mathbf{v}}^*_{zx}(\mathbf{x})\mathbf{j} + \check{\mathbf{D}}^k_{zy}\tilde{\mathbf{v}}^*_{zy}(\mathbf{x})\mathbf{k} \\ \check{\mathbf{C}}^k_{xy}\tilde{\mathbf{v}}(\mathbf{x}) &= \check{\mathbf{D}}^k_{xy}\tilde{\mathbf{v}}^*_{xy}(\mathbf{x})\mathbf{k} \end{aligned}$$

No interpolation is required and it can be generalized to a computational implementation for any order of accuracy. Notice that for 1D domains, the curl collapses to a divergence except that shifted.

In terms of future work, we suggest to compute the curl of:

$$\mathbf{v} = (\mathbf{i}+\mathbf{j}+\mathbf{k}) \times (\mathbf{i}x+\mathbf{j}y+\mathbf{k}z) = \mathbf{i}(z-y)+\mathbf{j}(x-z)+\mathbf{k}(y-x). \tag{27}$$

In this case, curl $\mathbf{v}(x,y,z) = 2\mathbf{i}+2\mathbf{j}+2\mathbf{k}$, which is constant throughout the entire 3D grid.

Then, we want to integrate this to the **The Mimetic Methods Toolkit (MTK)**, an API for the intuitive implementation of Mimetic Finite Differences in scientific applications [8].

References

[1] E.J. Sanchez, P. Blomgren, and J.E. Castillo. On the Role of Constrained Linear Optimization to Construct Higher-Order Mimetic Divergence Operators (under review). *Journal of Computational and Applied Mathematics*, 2014.

[2] J.E. Castillo and R.D. Grone. A matrix analysis approach to higher-order approximations for divergence and gradients satisfying a global conservation law. *Siam J. Matrix Anal. Appl.*, 25:128–142, 2003.

[3] J.B. Runyan. A Novel Higher Order Finite Difference Time Domain Method Based on the Castillo-Grone Mimetic Curl Operator with Applications Concerning the Time-Dependent Maxwell Equations. Master's thesis, San Diego State University, 2011.

[4] J.E. Castillo and G.F. Miranda. *Mimetic Discretization Methods*. CRC Press, 1st edition, 2013. In press.

[5] J.C. Maxwell. A treatise on electricity and magnetism. II(530), 1873.

[6] Eduardo Sanchez. Visualizer for 2D Staggered Grids. `http://www.mathworks.se/matlabcentral/fileexchange/47084-visualizer-for-2d-staggered-grids`, 2014.

[7] H. Anton, I. Bivens, and S. Davis. *Calculus Multivariable*. John Wiley & Sons, Inc., Hoboken, New Jersey, 8th edition, 2005.

[8] E.J. Sanchez, C.P. Paolini, and J.E. Castillo. The Mimetic Methods Toolkit: An object-oriented {API} for Mimetic Finite Differences. *Journal of Computational and Applied Mathematics*, 270(0):308–322, 2014. Fourth International Conference on Finite Element Methods in Engineering and Sciences (FEMTEC 2013).